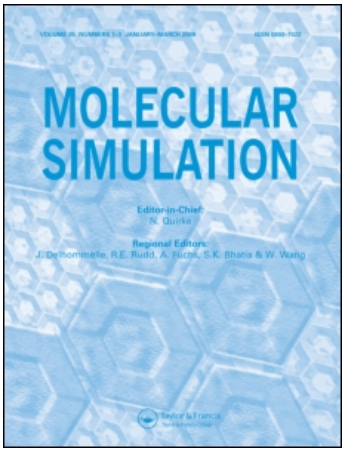

Molecular Simulation
Publication details, including instructions for authors and subscription information:
http://www.informaworld.com/smpp/title~content=t713644482

Zeolite microporosity studied by molecular simulation

Shuai Ban[a]; Thijs J. H. Vlugt[ab]
[a] Condensed Matter and Interfaces, Department of Chemistry, Utrecht University, TA Utrecht, The Netherlands [b] Process & Energy Laboratory, Delft University of Technology, CA Delft, The Netherlands

To cite this Article Ban, Shuai and Vlugt, Thijs J. H.(2009) 'Zeolite microporosity studied by molecular simulation', Molecular Simulation, 35: 12, 1105 — 1115
To link to this Article: DOI: 10.1080/08927020802660614
URL: http://dx.doi.org/10.1080/08927020802660614

Molecular Simulation
Vol. 35, Nos. 12–13, October–November 2009, 1105–1115

Taylor & Francis
Taylor & Francis Group

Zeolite microporosity studied by molecular simulation

Shuai Ban[a1] and Thijs J.H. Vlugt[b]*

[a]*Condensed Matter and Interfaces, Department of Chemistry, Utrecht University, TA Utrecht, The Netherlands;* [b]*Process & Energy Laboratory, Delft University of Technology, CA Delft, The Netherlands*

(*Received 8 October 2008; final version received 2 December 2008*)

A simulation method is presented to calculate efficiently the pore size distribution of microporous materials. The microporosity of several typical zeolites is analysed. The effects of the inaccessible pores and non-framework cations on the pore size distribution of zeolites have also been studied. Molecular simulations of Ar adsorption are used to investigate the correlations between the adsorption isotherms and the pore size distribution. The feasibility to derive the pore size distribution of zeolite micropores directly from adsorption isotherms is discussed.

Keywords: zeolites; microporosity; Argon adsorption; molecular simulation

1. Introduction

In recent years, major progress has been made in the synthesis and textual characterisation of highly ordered microporous materials, e.g. microporous molecular sieves [1–3]. Zeolites are important microporous molecular sieves with well-defined crystalline structures [4,5]. Therefore, the pore structure follows directly from the crystallographic data. Zeolite pores are narrow as the pore width is usually smaller than 1.5 nm. An accurate textural characterisation of microporous materials is of crucial importance for their application, e.g. in catalysis and separation technology [6–10]. The pore architecture, i.e. pore size, pore size distribution, pore volume, and pore topology all have a large influence on adsorption and transport phenomena [11–17]. Although many experimental methods are available for the characterisation of porous materials, physical adsorption is still the most popular one as it can access a wide range of pore sizes (from 0.35 to 100 nm) [18]. This includes the complete range from micro- and mesopores to macropores. Moreover, gas adsorption techniques are convenient to use and not cost intensive compared to some other methods such as small angle X-ray and neutron scattering, mercury porosimetry, electron microscopy, thermoporometry and NMR [18].

Physisorption occurs whenever a gas or liquid (the so-called 'guest') is brought into contact with the surface of a porous solid (host). The amount of adsorbed material (adsorption isotherm) is determined by the applied pressure and temperature, as well as the interplay between the guest–host and guest–guest interactions in the pores. This is reflected in the shape of the adsorption isotherm. The IUPAC classification of adsorption isotherms [19] distinguishes six types of isotherms. Pores are classified by their internal pore width (the pore width of a cylindrical pore is defined by its diameter; for slit pores the pore width is defined as the distance between opposite walls). Pores smaller than 2 nm are classified as micropores, while mesopores have a pore width between 2 and 50 nm. Pores larger than 50 nm are classified as macropores.

In order to extract the surface area, pore size, pore size distribution, pore volume, pore topology and porosity from gas adsorption isotherms, one needs to apply suitable theoretical models that capture the important underlying adsorption mechanisms. Molecular simulations (Monte Carlo and molecular dynamics) have been used to obtain a better understanding of sorption phenomena in porous materials [17,20–33]. These microscopic methods describe the guest–host system at a molecular level, in contrast to the classical methods that are based on macroscopic thermodynamics. It has been shown that the application of theoretical and molecular simulation-based methods leads to a much more accurate pore size analysis over the complete micro and mesopore size range [34–36].

In this work, we present an efficient simulation method to characterize zeolite pores in terms of the micropore size distribution, the micropore volume and the accessibility of micropores. Only the coordinates of the zeolite framework atoms are required, and they can be derived from XRD experiments easily. The details of our approach are presented in Section 2. In Section 3, we briefly discuss the pore size distribution of some typical zeolites, and show how this is affected by non-framework cations. We also briefly discuss the fact that for some zeolite structures, some parts are inaccessible. For various framework structures, we study the physisorption of Ar using

*Corresponding author. Email: t.j.h.vlugt@tudelft.nl

ISSN 0892-7022 print/ISSN 1029-0435 online

DOI: 10.1080/08927020802660614
http://www.informaworld.com

Monte Carlo simulations in the grand canonical ensemble. Several models are discussed on how to relate the isotherm of Ar adsorption to the pore size distribution. Concluding remarks will be given in Section 4.

2. Simulation methods

2.1 Pore size distribution

In this work, the pore size of a certain cavity is defined as *the maximum diameter of a sphere that can be located in that cavity.* This definition is applicable to pores with an arbitrary shape. For cylindrical or slit pores, our definition is identical to the IUPAC definition. Using our definition of the pore size, the pore size distribution is computed from the coordinates of the framework atoms using the algorithm shown in Figure 1: (1) a three-dimensional grid with a small spacing is constructed. We typically use a grid size of 0.1 Å (in each direction). (2) A spherical test particle is positioned at a random position in the zeolite. The radius of this particle is chosen as the minimum distance between the centre of the particle and any of the zeolite framework atoms, minus the radius of the closest framework atom. The radius of an oxygen framework atom is 1.35 Å. Tetrahedral atoms, e.g. Si, Al, are not considered as for most zeolites they are well screened by adjacent oxygen atoms [37]. (3) The diameter of the test particle is recorded for all grid points that are inside the test particle. (4) This procedure is repeated many times. We found that the number of test spheres should be at least 100 times the number of grid points. For each grid point, the maximum recorded diameter is computed and this quantity is defined as the local pore size of a specific grid point. The simulation stops when the local pore size of all grid points is converged. (5) The fraction of pores with a diameter between r and $r + \Delta r$ (pore size distribution) is equal to the fraction of grid point with a maximum diameter between r and $r + \Delta r$. Note that the channel dimensions of zeolites suggested by Atlas of Zeolite Structures [38] are actually the sizes of the channel openings, directly related to the accessibility. This definition of pore size is slightly different compared with ours.

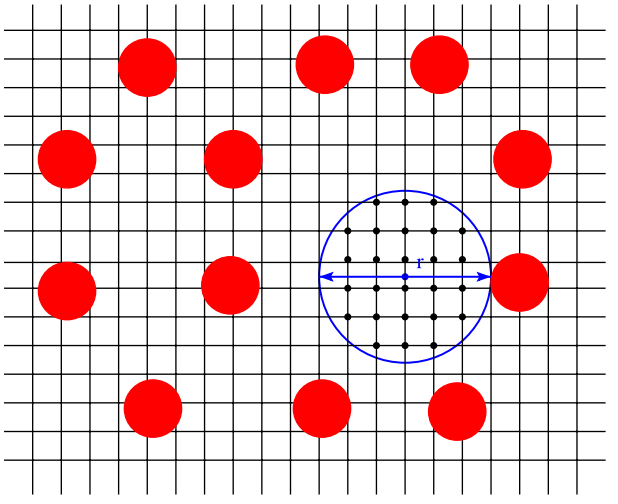

Figure 1. Schematic representation of the simulation scheme to compute the pore size distribution of porous materials. The red spheres are the zeolite atoms, and the blue circle represents the particle inserted randomly in the zeolite framework. The black dots are the grid points inside the inserted particle with a diameter r.

N_2/Ar physisorption experiments are the most often methods used to measure the total pore volume experimentally. These methods can only detect the pores larger than 4.5 Å [2]. Using our calculated pore size distribution, the micropore volume is calculated by integrating the pore size distribution up to 20 Å, starting from pore sizes of 4.5 or 3.5 Å. It is important to note that some zeolites (e.g. LTA-type zeolite) may contain inaccessible cavities, that are (in principle) large enough to accommodate adsorbate molecules. In this case, the largest entrance to the cavities is often a small six-membered ring. The contribution of the inaccessible cavities to the total micropore volume should be subtracted, depending on the size of the guest molecules. In this work, we will try to establish a relationship between the pore size distribution and adsorption isotherms computed using molecular simulations. Therefore, to make this comparison it is not necessary to artificially block inaccessible cages. However, for a comparison between computed isotherms and measured isotherms one needs to take care that in the simulations, the inaccessible cages are really inaccessible for guest molecules.

2.2 Ar physisorption

Gas physisorption is the most popular method for the characterisation of pore sizes as it allows accessing a wide range of pore sizes (from 0.35 to 100 nm). Ar shows nearly perfect physisorption behaviour at cryogenic conditions (87.3 K) [19]. Compared to N_2 and CO_2, Ar has weaker attractive interactions with the host structure, in particular for zeolites with non-framework cations [39]. As a consequence, micropores of 0.5–1 nm are filled with Ar at much higher relative pressures, i.e. $10^{-5} < p/p_0 < 10^{-3}$ than for N_2 (p_0 being the saturation pressure). However, analysis of Ar physisorption is problematic for small zeolite micropores. The reason for this is that when the pore size is close to the kinetic diameter of Ar, the local density of Ar inside zeolite micropore becomes smaller than the density of liquid Ar due to confinement effects. Therefore, the pore volume cannot be computed directly from the density of liquid Ar as this will lead to an underestimation of the micropore volume.

In this study, simulations of Ar adsorption in zeolites at 77 K are conducted. This will be used to develop the correlation between the Ar adsorption isotherms and the simulated micropore size distributions. Adsorption

isotherms are calculated using Monte Carlo (MC) simulations in grand canonical (GC) ensemble (for details we refer the reader to [40–43]). Lennard-Jones (LJ) interactions are used to describe interactions between Ar and zeolite atoms. The intermolecular interactions are truncated and shifted at 12 Å [44]. Periodic boundary conditions in all directions are applied. The pressure is varied between 10^{-5} and 10^{2} kPa at 77 K. A typical simulation consists of at least 2×10^{6} cycles. In each cycle, trial moves are attempted to translate or to exchange a molecule with the reservoir [42]. The number of trial moves per cycle is equal to the number of molecules with a minimum of 20. As we want to make a comparison between the computed pore size distribution and the computed adsorption isotherms, it is not necessary to identify or block inaccessible cages. We would like to point out that for comparison with experimental isotherms it is necessary to block inaccessible cages in the simulations.

In our simulations, the zeolites are considered rigid as framework flexibility only results in very small deviations of adsorption properties [45]. For MFI-type zeolite, however, a phase transition of the zeolite framework may occur upon Ar adsorption [46–50]. A detailed study of this is beyond the scope of the present work. In our adsorption simulations, all zeolites are considered as all-silica structures. The LJ interaction parameters are chosen as $\sigma_{Ar—Ar} = 3.42$ Å, $\varepsilon_{Ar—Ar}/k_B = 124.07$ K, $\sigma_{Ar—O} = 3.17$ Å and $\varepsilon_{Ar—O}/k_B = 95.61$ K [51]. The LJ interaction between Si and Ar is not taken into account [52].

The Dubinin–Astakhov (DA) adsorption equation was used to model the filling of a pore of diameter r [53]:

$$N(r,p) = \rho(r)\exp\left[-\left(\frac{RT\ln(p_0/p)}{\alpha E_0(r)}\right)^{n(r)}\right] \qquad (1)$$

in which $N(r,p)$ is the loading of adsorbed molecules at pressure p, ρ (in units of mmol/ml) is the saturation loading of Ar in pores of diameter r, $P(r)$ is the pore size distribution in units of ml/g^{-1} Å^{-1}, α is the (dimensionless) affinity parameter (0.31 for Ar [53]), E_0 is the characteristic adsorption energy (kJ/mol), p_0 is the saturation vapour pressure, and $n(r)$ is a constant that only depends on r. The total loading $\theta(p)$ of Ar in the zeolite is computed by integration over all pores [35,36,54–56],

$$\theta(p) = \int_{r=3.5\,\text{Å}}^{r=20\,\text{Å}} P(r')N(r',p)\mathrm{d}r'. \qquad (2)$$

This integration is from the minimum considered pore diameter 3.5 Å to the maximum pore diameter of micropores (20 Å). In total, three parameters in Equation (1) depend on the pore diameter r: $\rho(r)$, $E_0(r)$ and $n(r)$. The function $\rho(r)$ determines the saturation loading at which the adsorption isotherm levels off. The adsorption energy $E_0(r)$ determines at which pressure the guest molecules start to enter the zeolite cavities. The function $n(r)$ defines the slope of the isotherm prior to saturation.

For a large collection of zeolites, we have fitted $\rho(r)$, $E_0(r)$ and $n(r)$ using the pore size distribution computed using the scheme described in Section 1. This is done as follows. (1) For zeolites with only one pore type or adsorption site, the value of $\rho(r)$ can be computed directly from the pore volume and the saturation loading. Some care is needed for zeolites with more than one pore type. In this case, we identify the number of adsorption sites by the inflection behaviour of the adsorption isotherm [57,58]. If the inflection behaviour is absent, then we only consider a single adsorption site. Inflection behaviour of the adsorption isotherm is not necessarily caused by the presence of multiple adsorption sites, as it may also be caused by rearrangement of the guest molecules. Simulation snapshots have been used to identify whether or not multiple adsorption sites are present. (2) The other parameters $E_0(r)$ and $n(r)$ are fitted to the computed adsorption isotherm. (3) The fitting procedure is repeated for many zeolites and we will investigate general trends in the obtained values for $\rho(r)$, $E_0(r)$ and $n(r)$.

From the functions, $\rho(r)$, $E_0(r)$ and $n(r)$, now fitted for all zeolites, we will investigate whether or not it is possible to predict the earlier computed pore size distribution from the computed adsorption isotherm. This is done as follows. For pore diameters r in the range (4–13 Å), the corresponding pore volume equals $\theta(p_0)/\rho(r)$. We compute the absolute error between the computed isotherm (using GCMC) and the fitted isotherm (calculated using Equations (1) and (2) and the functions $\rho(r)$, $E_0(r)$ and $n(r)$ fitted for all zeolites simultaneously). The pore diameter that leads to the smallest difference is selected. For zeolites with more than one adsorption site, the simulated Ar adsorption isotherm is separated using the inflection pressure corresponding to the adsorption of Ar in different pore types. The pore diameters that lead to the smallest difference between the computed and fitted isotherm are selected.

3. Results and discussions

3.1 Micropores of all-silica zeolites

The pore size distributions have been computed for most of the zeolite structures taken from IZA zeolite database [38]. The total micropore volume is calculated by integrating the pore size distribution in the range of pore diameters 3.5–20 Å and 4.5–20 Å. Results for typical all-silica zeolites are listed in Table 1. It is trivial to see that the pore volume integrated from 3.5 Å ($V_{3.5}$) is slightly larger than the pore volume integrated from 4.5 Å ($V_{4.5}$). In particular, MON-type zeolite has an unique 4 Å pore, which leads to $V_{4.5} = 0$.

Detailed information of the zeolite porosity for BEA, MFI and RHO can be seen in the pore size distributions and the corresponding contours in Figure 2. Zeolite BEA

Table 1. Micropore volumes of various all-silica zeolites computed using the scheme described in Section 2.1.

Zeolite type	$V_{3.5}$ (ml/g)	$V_{4.5}$ (ml/g)	Zeolite type	$V_{3.5}$ (ml/g)	$V_{4.5}$ (ml/g)
AEL	0.136	0.126	AET	0.172	0.165
AFI	0.192	0.184	AFO	0.129	0.119
AFR	0.341	0.280	AFS	0.405	0.366
AFY	0.489	0.452	ATN	0.179	0.149
ATO	0.118	0.107	BEA	0.322	0.314
BOG	0.299	0.286	BPH	0.289	0.273
CHA	0.357	0.332	EAB	0.299	0.281
EUO	0.192	0.179	FER	0.225	0.210
GME	0.357	0.315	KFI	0.344	0.315
LEV	0.324	0.303	LTN	0.304	0.261
MAZ	0.282	0.221	MEI	0.387	0.351
MEL	0.210	0.198	MER	0.308	0.120
MFI	0.211	0.201	MFS	0.199	0.164
MON	0.200	0.000	MOR	0.238	0.208
MTT	0.126	0.106	MWW	0.270	0.253
OFF	0.301	0.289	RHO	0.381	0.350
TON	0.134	0.121	VFI	0.337	0.328
AWW	0.246	0.230	CAN	0.247	0.136
DDR	0.249	0.226	ERI	0.293	0.281
EMT	0.452	0.439	FAU	0.481	0.468
LTA	0.457	0.440	LTL	0.211	0.203

Zeolite framework coordinates were taken from the IZA zeolite database [38]. V_x denotes the micropore volume calculated in the range $x-20$ Å. Zeolites in the bottom table contain cages that are inaccessible for most guest molecules. To calculate the density of the zeolite (in g/ml), all framework atoms other than Si have been replaced by Si. Note that this only influences the value for the pore volume per gram zeolite, and not the pore volume per unit cell. Non-framework cations have not been considered here.

has two different channels running along the crystallographic *x*- and *y*-axis, respectively. The sizes of these channel openings are 6.6×6.7 and 5.6×5.6 Å. The simulated pore size distribution for zeolite BEA in Figure 2(a) shows a slightly disperse pore size ranging from 6.25 to 6.55 Å, corresponding to the channel interiors shown from the contour plot. In Figure 2(b), the pore size distribution of MFI shows a large peak at 6.7 Å and some smaller ones between 5.4 and 5.7 Å. The corresponding contour map suggests that the large peak corresponds to the intersections of the straight channel (5.3×5.6 Å) and the zigzag channel (5.1×5.5 Å). Peaks in the range of 5.4–5.7 Å represent the channel interiors of MFI. The RHO-type framework has a cage-like structure, where large *Ita* cages are connected by small eight-membered rings (3.6×3.6 Å). The pore size distribution of RHO shows two sharp peaks at a pore diameter of 12 Å and 4.5 Å, respectively. The corresponding contour map indicates that the cage interiors with a pore diameter 12 Å and the small windows in size of 4.5 Å have the largest contribution to the pore volume.

As mentioned earlier, the zeolite framework may contain inaccessible cages that consist of six-membered (or smaller) rings. As the six-membered opening is smaller than 3 Å, it will prevent most molecules with a kinetic diameter larger than 3 Å to enter the cage. The LTA zeolite has two types of cages: (1) the *sod* cage consisting of four- and six-membered rings and (2) the *ita* cage possesses extra eight-membered rings that make it accessible [38]. From the contour map in Figure 3(b), it can be seen that there are four *sod* cages located in the centre, edges and corners on the $y-z$ slice of a LTA unit cell. The pore size distribution in Figure 3(a) shows two pores of diameters 6.5 and 11.3 Å, corresponding to the interiors of the inaccessible *sod* cage and the accessible *ita* cages. The total pore volume larger than 3.5 Å equals 0.457 ml/g. This volume decreases to 0.347 ml/g when the contribution of the *sod* cage is excluded.

Compared to all-silica zeolites, many zeolites have much more complex compositions, as they may contain framework atoms like Al, P, Co and non-framework compounds like Li, Na, Ca, Mg and H_2O, etc. Non-framework cations occupy a certain volume and therefore they influence the pore size distribution. Figure 4 shows the effect of non-framework Na cations on the pore size distribution of Na-MOR framework in the *Pbcn* space group. The framework of MOR consists of two distinct cavities, which are 12-membered main channels (7.0×6.5 Å) in the direction of the *z*-axis and eight-membered side pockets (3.4×4.8 Å) in *y* direction [38]. In Na-MOR, the adsorption of guest molecules is very sensitive to the distribution of aluminium atoms [59,60]. In our present study, we randomly distribute Al atoms over all tetrahedral sites of the Na-MOR supercell, in such a way that the Löwenstein rule as well as the guidelines outlined by Alberti [61] are satisfied. This fixes the Al content for each of the crystallographic T-sites in MOR-type zeolite. The pore size distribution of all-silica MOR (*Pbcn*) has two major peaks at pore diameters of 4.5 and 5.9 Å, corresponding to the side pocket and the main channel (see Figure 5(a)). When non-framework Na cations are present, both peaks become 60% lower than those of the all-silica MOR, while some minor peaks appear at smaller pore diameters around 4.2 and 5.7 Å. The reason for this is that non-framework Na cations make the pore less uniform. This can be seen from Figure 5(b). This figure also shows that non-framework Na cations sitting near the opening of the side pockets partially or fully block the entrance of the side pockets, and narrow the main channels to some extent. The pore volume ($V_{3.5}$) of the all-silica MOR is 0.199 ml/g ($0.35V_{\text{unitcell}}$) and that of Na-MOR decreases to 0.176 ml/g ($0.327V_{\text{unitcell}}$, V_{unitcell} being the volume of the unit cell). This indicates that the non-framework Na cations occupy the void space of zeolites and cause a volume loss of $0.023V_{\text{unitcell}}$. For a fixed Al content of the four T-sites, we found only very small differences in the total pore volume for different distributions of Al atoms. However, for a different Al content of the T-sites, the pore volume will be different due to a different fraction of Na in the side pockets.

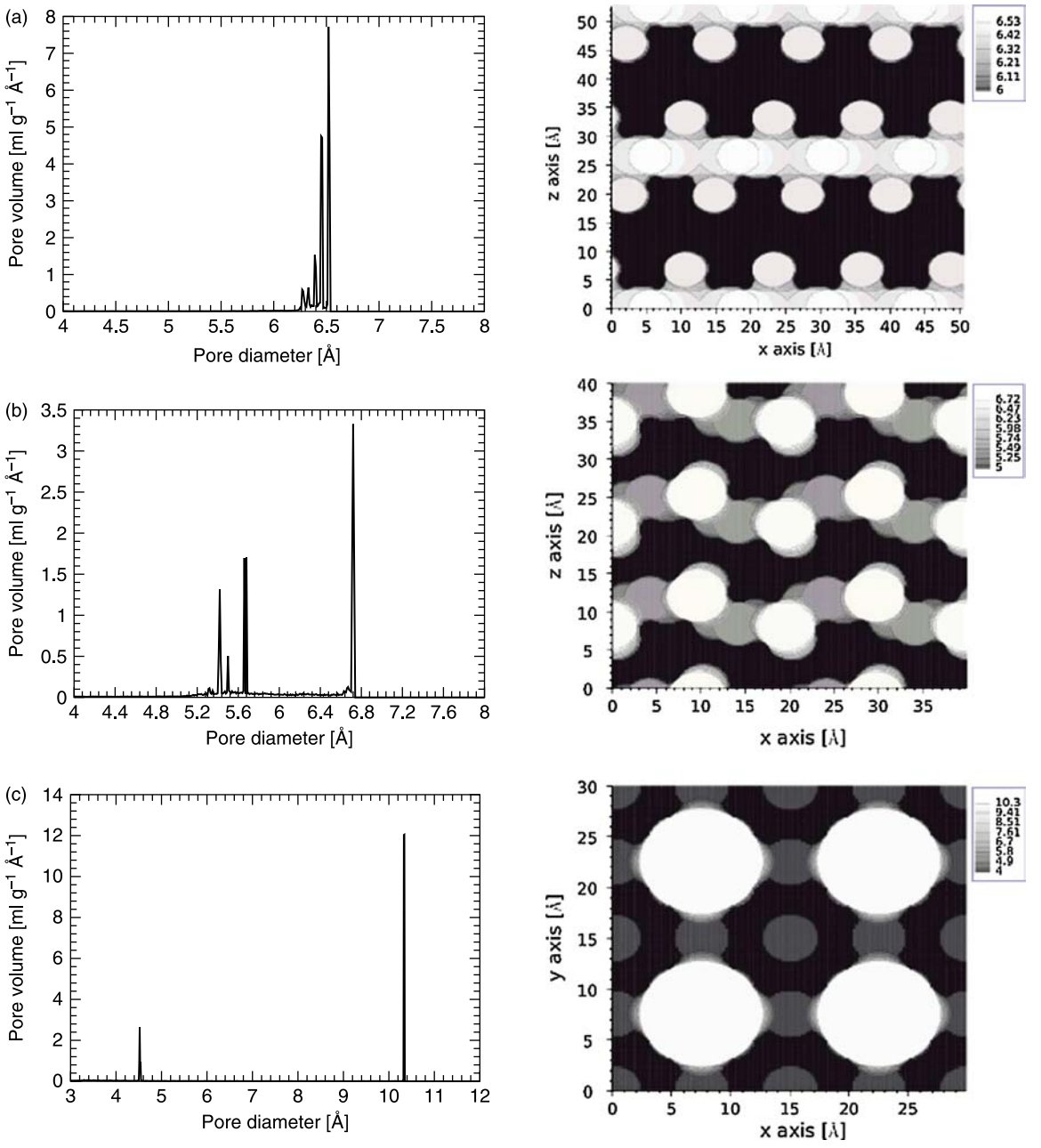

Figure 2. Left: Computed pore size distributions of various zeolites: (a) BEA, (b) MFI and (c) RHO. Right: Corresponding contour plots for BEA, MFI and RHO. The contour planes are chosen as follows: x–z plane at $y = 0.75b$ for BEA, x–z plane at $y = 0.25b$ for MFI and x–y plane at $z = 0.5c$ for RHO (a,b,c being the length of the basis vectors of the unit cell). The colour of the contour maps denotes the pore diameter. The dark area in the contour plots denotes cavities with a pore diameter smaller than 6 Å for BEA, pore diameters smaller than 5 Å for MFI and pore diameter smaller than 4 Å for RHO.

3.2 Ar physisorption

The computed adsorption isotherm of Ar in MFI-type zeolite at 77 K is plotted in Figure 6, along with its fit to Equations (1) and (2). The computed adsorption isotherm shows an inflection point at 0.01 kPa. The pore size distribution in Figure 2 shows that MFI has two different pores at 5.5 and 6.7 Å, corresponding to the channel interiors and channel intersections, respectively. In principle, from the isotherm only, one may relate the inflection to different adsorption capacities of different adsorption sites. However, a simulation snapshot of Ar at 0.01 kPa (Figure 6) shows that both the channel interiors and intersections are simultaneously filled by Ar molecules. The step-like behaviour of the Ar adsorption

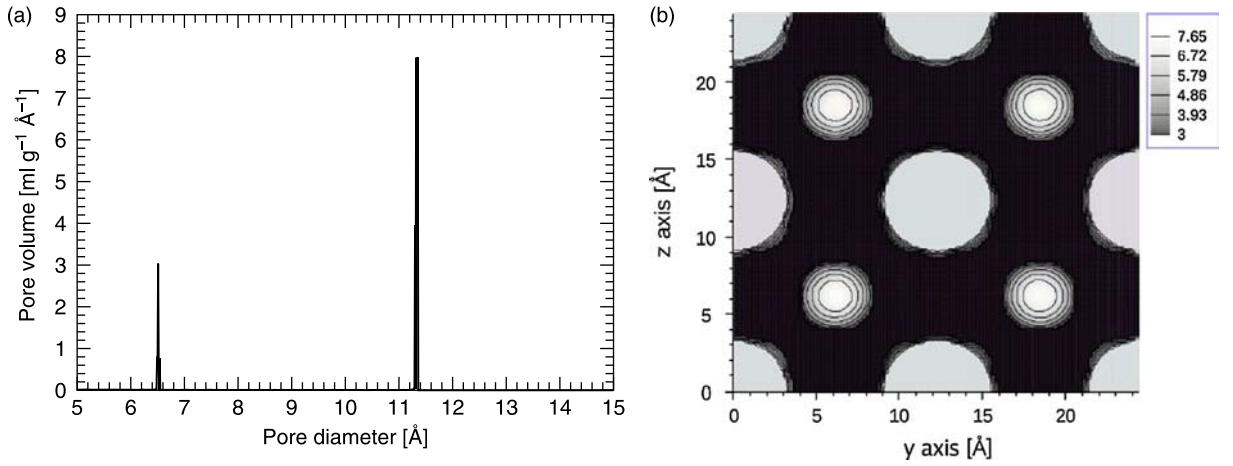

Figure 3. (a) Computed pore size distribution and (b) the contour map for the LTA-type zeolite. The contour plane is chosen as the y–z plane at $x = 0.5a$. The colour of the contour maps denotes the pore diameter. The dark area in the contour plot denotes cavities with a pore diameter smaller than 3 Å.

isotherm in these simulations is therefore not caused by the Ar adsorption in *different* pores of MFI [46]. Therefore, it is convenient here to consider MFI as a zeolite containing a single adsorption site. The fitted isotherm agrees well with the isotherm for simulations. The fitting parameters are $\rho = 26.33$ mmol/ml, $E_0 = 21.21$ kJ/mol and $n = 4.24$ at the selected diameter 5.7 Å. The typical pore diameter is chosen from the major peaks of the pore size distribution, which covers the largest pore volume.

The typical fitting results for Ar adsorption in zeolite CAN at 77 K are shown in Figure 7. Similar to MFI, the adsorption isotherm of Ar in CAN shows two inflection points at the pressure of 10^{-4} and 1 kPa, respectively.

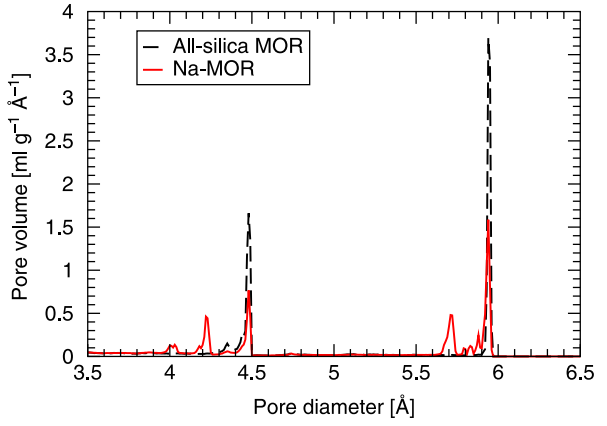

Figure 4. Simulated pore size distributions for all-silica MOR and Na-MOR with Si/Al = 5. The pore size distribution of Na-MOR is obtained by averaging 10 Na-MOR samples with Si/Al = 5. The non-framework Na cations are preferentially located at three adsorption sites: the main channels, the opening of the side pocket and the eight-membered rings [62,63].

The snapshots of the simulations (Figure 8) confirm that the first inflection point at 2.5×10^{-4} corresponds to saturation of the small *can* cages (4.3 Å), while the second inflection at 1 kPa is attributed to the packing of Ar in the large channels along the z-axis. Therefore, two different DA isotherms are used to fit the complete isotherm. For the *can* cages, the fitted parameters are $\rho = 11.61$ mmol/ml, $E_0 = 32.21$ kJ/mol and $n = 17.31$ using a pore diameter of 4.3 Å. For the large channel, the fitted parameters are $\rho = 22.40$ mmol/ml, $E_0 = 19.15$ kJ/mol and $n = 3.60$ for a pore diameter of 6.3 Å. By comparing the two sets of DA parameters, it can be seen that the large channel always has a higher loading capacity but weaker adsorption strength than the small pore. Note that the parameter n is much more sensitive to the pore shape and the molecular packing than the other parameters.

This fitting of computed isotherms to Equations (1) and (2) was conducted for nearly 40 zeolite framework types. The collection of the fitted DA parameters in the range of 4–13 Å is shown in Figure 9. In Figure 9(a), the general trends can be identified for $\rho(r)$ and $E_0(r)$. Fluctuation in their values is caused by the dependence of the zeolite adsorption on the pore shapes and the molecular packing.

Starting from a pore diameter of $r = 4$ Å, $\rho(r)$ has a sharp increase of up to 25 mmol/ml at 6 Å followed by a slow convergence to 33 mmol/ml at the pore diameter 13 Å. Furthermore, at the maximum micropore diameter 20 Å, $\rho = 35.6$ mmol/ml, which agrees well with the standard density of the liquid Ar (35.8 mmol/ml). This means that Ar will stay in the liquid phase when the pore is large enough. However, for zeolite micropores smaller than 20 Å, calculation of the micropore volume using the density of liquid Ar (35.8 mmol/ml) will result in an underestimation of the pore volume up to about 30%.

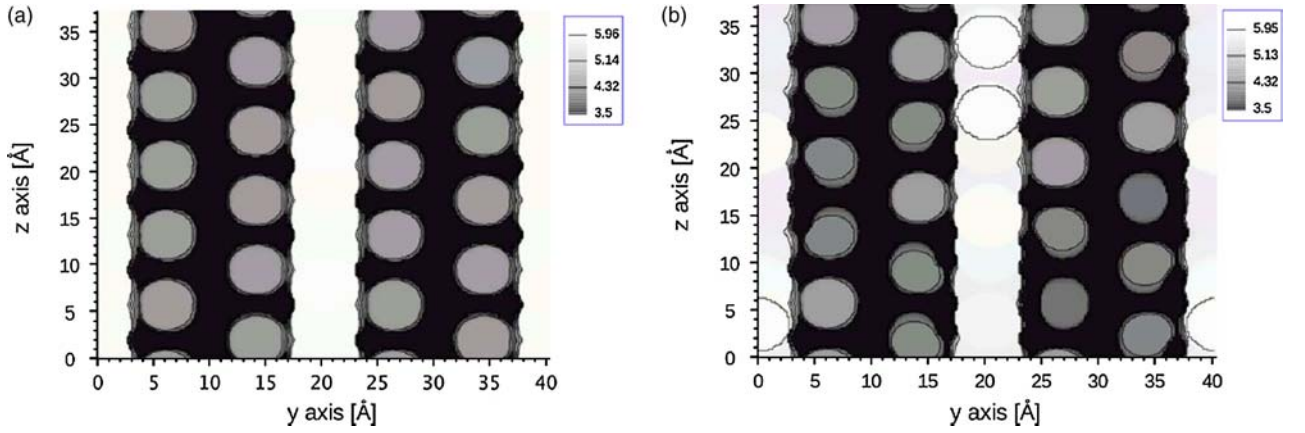

Figure 5. (a) Typical snapshots of simulated contours for the all-silica MOR and Na-MOR with Si/Al = 5. The contour planes are chosen as the y–z plane at $x = 0.5a$. The colour of the contour maps denotes the pore diameter. The dark area in the contour planes denotes cavities with a pore diameter smaller than 3.5 Å.

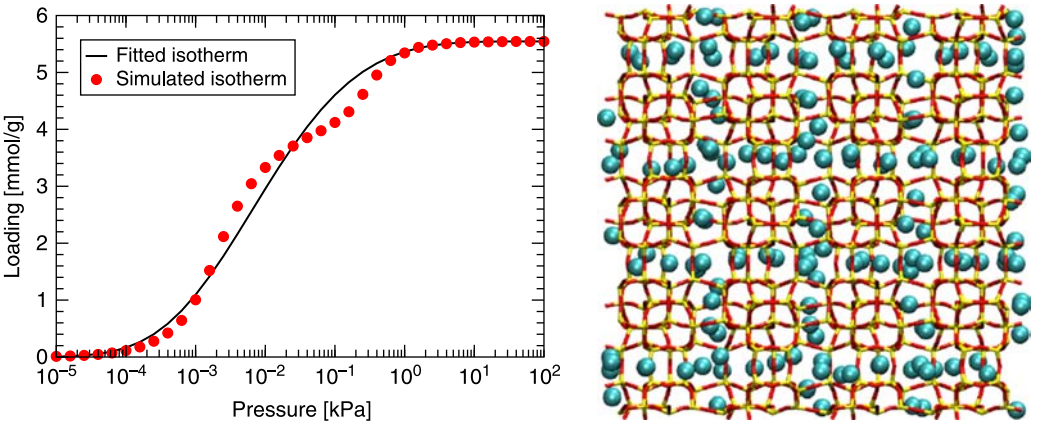

Figure 6. Left: Adsorption isotherms of Ar in MFI-type zeolite, along with a fit to Equations (1) and (2). Right: Typical snapshot (x–y plane) at 0.01 kPa at 77 K.

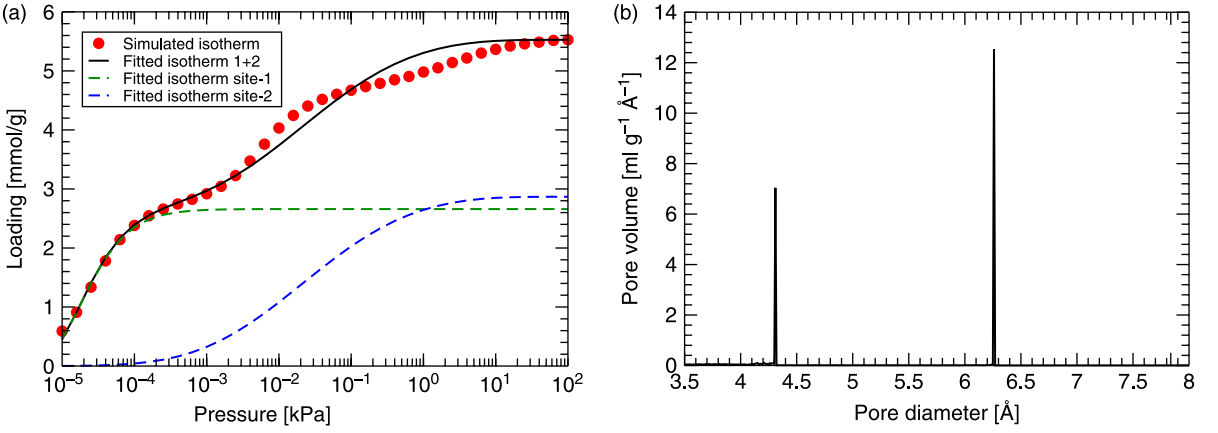

Figure 7. Left: Simulated adsorption isotherms of Ar in CAN at 77 K. The dashed lines are the fitted isotherms for the two distinct adsorption sites. Right: The calculated pore size distribution of CAN. The blocking of the inaccessible cages is not considered.

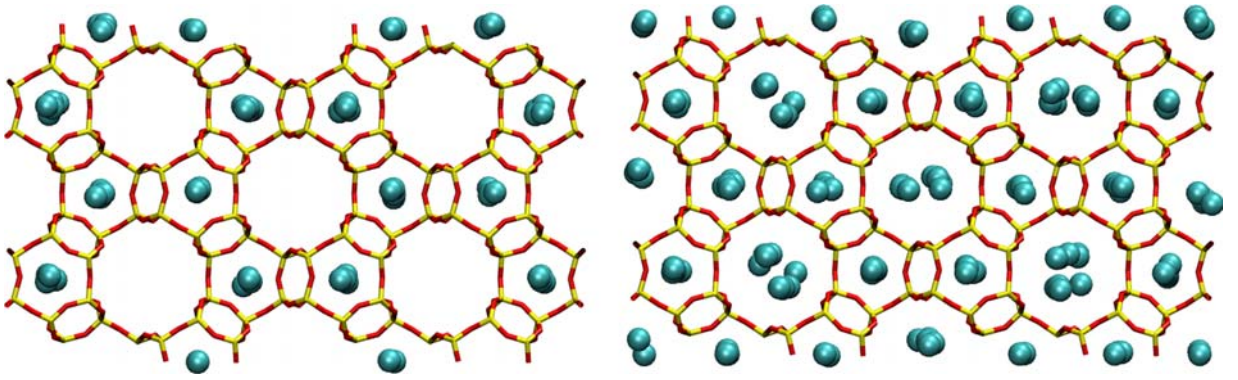

Figure 8. Typical snapshots (x–y plane) of Ar adsorbed in CAN-type zeolite at a pressure of 2.5×10^{-4} kPa (left) and 10^{2} kPa (right). The blocking of the inaccessible cages is not considered.

For the adsorption energy $E_0(r)$, a reverse trend can be observed. Starting from a large adsorption energy of 34 kJ/mol at $r = 4$ Å, E_0 gradually decreases and levels off around 15 kJ/mol at the diameter 13 Å. This is because small pores have a stronger adsorption strength than large pores. The slope parameter $n(r)$ plotted in Figure 9(b) shows a larger scatter due to the large sensitivity on the adsorption isotherm.

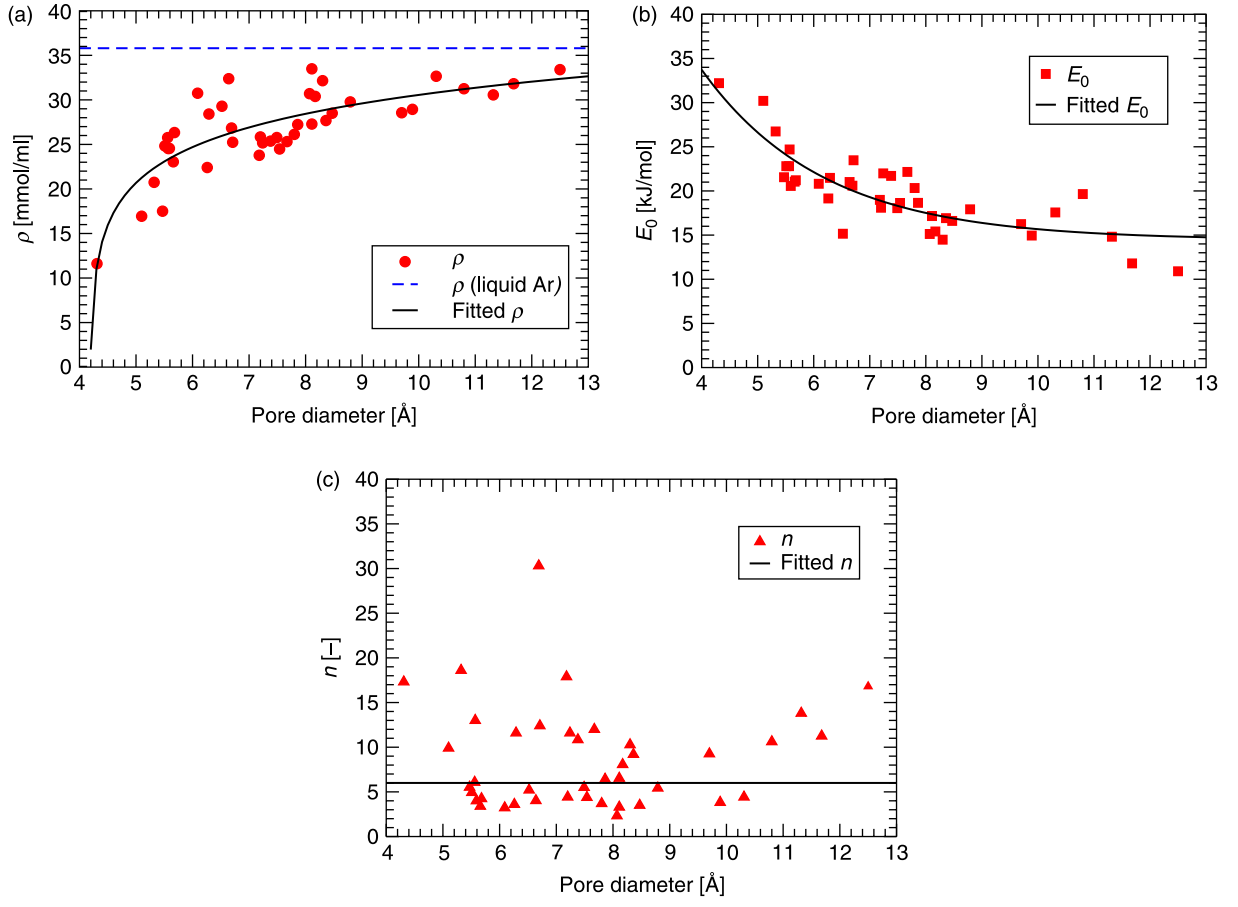

Figure 9. The fitted parameters for the DA adsorption isotherm, i.e. ρ, E_0 and n, as a function of the pore diameter in the range from 4 to 13 Å for various zeolites. In (a), the density ρ of the liquid Ar (35.8 mmol/ml) is drawn as a dashed line.

The collected DA parameters in the range of 4–13 Å for Ar at 77 K can be fitted using:

$$\rho(r) = 5.04 \ln[r - 4.18] + 21.68, \quad (3)$$

$$E_0(r) = 121.37 \exp[-0.46r] + 14.45, \quad (4)$$

$$n(r) = 6, \quad (5)$$

in which r is the pore diameter in Å, ρ and E_0 are in units of mmol/ml and kJ/mol, respectively. From the concentration parameter $\rho(r)$ in Equation (3), it can be seen that the minimum pore diameter that can be estimated from the Ar adsorption isotherm is about 4 Å, and any pores smaller than that exceed the measurement capability of the Ar physisorption.

Using the fitted DA adsorption parameters of Equations (3)–(5), we recomputed the pore volume and pore size of zeolites directly from the computed Ar adsorption isotherms, and compared the results with the direct computation using the algorithm described in Section 1. Nearly 40 framework types have been tested in this way (see Table 2). For most zeolites, the pore volume and size are correctly reproduced compared to the pore size distributions simulated earlier (using the method of Section 1). In general, this procedure is more accurate for zeolites containing a single adsorption site than for zeolites containing multiple adsorption sites. For the latter, the difficulty is that the adsorption isotherms may contain inflections corresponding to the self packing of Ar. To identify the number of the adsorption sites prior to fitting the adsorption isotherms requires

Table 2. Comparison of fitted pore volumes (V) and pore sizes (r) and the calculated ones for various all-silica zeolites.

Zeolite type	Adsorption sites	Fitted V (ml/g)	Calculated $V_{3.5}$ (ml/g)	Fitted r (Å)	Calculated r (Å)
AEL	1	0.142	0.136	5.6	5.6
AET	1	0.170	0.172	13.0	8.3
AFI	1	0.179	0.192	8.7	8.1
AFO	1	0.138	0.129	5.8	5.6
AFR	2	0.397	0.341	4.8, 9.6	4.4, 8.1
AFS	1	0.375	0.405	9.5	9.7
AFY	1	0.477	0.489	8.0	8.5
ATN	1	0.182	0.179	5.4	5.7
ATO	1	0.083	0.118	6.1	5.5
AWW	1	0.231	0.246	6.2	7.4
BEA	1	0.301	0.322	10.9	6.5
BOG	2	0.270	0.299	5.2, 7.7	7.2, 8.4
BPH	1	0.307	0.289	7.7	8.8
CAN	2	0.324	0.247	4.4, 8.4	4.3, 6.3
DDR	1	0.291	0.249	5.8	7.7
EAB	1	0.268	0.299	7.2	7.5
EUO	1	0.246	0.192	5.9	6.7
FAU	1	0.439	0.481	13.0	11.7
FER	1	0.235	0.225	5.7	5.5
GME	2	0.350	0.357	5.3, 7.9	5.0, 7.9
KFI	1	0.399	0.344	7.0	10.8
LEV	1	0.304	0.324	7.4	7.2
LTA	1	0.393	0.457	13.0	11.3
LTL	1	0.201	0.211	9.7	9.9
MAZ	2	0.267	0.282	5.2, 7.3	6.3, 8.1
MEI	1	0.396	0.387	9.1	8.2
MEL	1	0.204	0.210	6.2	5.6
MER	1	0.392	0.308	5.8	6.1
MFI	1	0.225	0.211	6.0	5.7
MFS	1	0.186	0.199	6.1	6.6
MTT	1	0.173	0.126	5.8	5.6
MOR	2	0.274	0.238	4.6, 7.5	5.1, 6.7
MWW	1	0.282	0.270	6.1	7.8
OFF	1	0.280	0.301	7.5	7.5
RHO	2	0.437	0.381	5.0, 9.8	4.5, 10.3
TON	1	0.125	0.134	5.3	5.3
VFI	1	0.345	0.337	13.0	12.5

The calculated pore volume $V_{3.5}$ is calculated using the algorithm described in Section 2.1. The fitted pore volume is obtained by fitting Equations (1) and (2) to the adsorption isotherms (computed from GCMC simulations) using Equations (3)–(5) for ρ, E_0 and n. The pore diameters are obtained in a similar way. Note that the MOR-type framework has space group *Cmcm*.

knowledge of the zeolite structure. Many zeolites may be subject to some severe chemical pretreatments. These can amorphise the zeolite framework into a less well-defined structure.

4. Conclusions

A method to characterise the zeolite microporosity has been developed. The pore volume and the pore size distribution of zeolites can be computed accurately. The contour maps of zeolites clearly show the position and diameter of the zeolite pores. In this way, it is possible to easily identify the locations and the local pore volume of the inaccessible cages for some zeolites. The simulations of Na-MOR show that the non-framework Na cations may occupy the internal space and cause a decline for both the pore volume and the pore size compared to all-silica frameworks.

Based on the calculated pore size distributions for various zeolites, adsorption isotherms of Ar have been fitted by the DA equations. The collection of three DA parameters shows clear trends as a function of the pore diameter. By using fitted functions for all three DA parameters, it is possible to identify the pore volumes and the pore sizes directly from the corresponding Ar adsorption isotherm. The fitted results of zeolite microporosities agree well with the ones directly calculated.

Acknowledgements

The authors acknowledge funding from the ACTS/ASPECT programme from The Netherlands Organisation for Scientific Research (NWO-CW). T.J.H. Vlugt acknowledges financial support from NWO through a VIDI grant.

Note

1. Email: s.ban@tudelft.nl

References

[1] J. Cejka and H. van Bekkum (eds.), *Zeolites and Ordered Mesoporous Materials: Progress and Prospects*, Elsevier, Amsterdam, 2005.
[2] J. Cejka, H. van Bekkum, A. Corma, and F. Schüth (eds.), *Introduction to Zeolite Science and Practice 3th*, Elsevier, Amsterdam, 2007.
[3] M. Lu and X.S. Zhao (eds.), *Nanoporous Materials: Science and Engineering*, Imperial College Press, London, 2004.
[4] D.W. Breck, *Zeolite Molecular Sieves*, Wiley, New York, NY, 1974.
[5] R.M. Barrer, *Zeolites and Clay Minerals as Sorbents and Molecular Sieves*, Academic Press, London, 1979.
[6] A. Bouyermaouen and A. Bellemans, *Molecular dynamics simulation of the diffusion of* n*-butane and* i*-butane in silicalite*, J. Chem. Phys. 108 (1998), pp. 2170–2172.
[7] L.A. Clark, *Confinement and pore shape effects on adsorption, diffusion and reaction in zeolites*, Ph.D. thesis, Northwestern University, Evanston, IL, USA, 2000.
[8] P. Demontis, E.S. Fois, G.B. Suffritti, and S. Quartieri, *Molecular dynamics studies on zeolites. 4. Diffusion of methane in silicalite*, J. Phys. Chem. 94 (1990), pp. 4329–4334.
[9] S. Gupta, S.S. Nivarthi, A.V. McCormick, and H.T. Danish, *Evidence for single file diffusion of ethane in the molecular sieve $AlPO_4$-5*, Chem. Phys. Lett. 247 (1995), pp. 596–600.
[10] B. Smit and T.L.M. Maesen, *Towards a molecular understanding of shape selectivity*, Nature 451 (2008), pp. 671–678.
[11] V.A. Harmandaris, D. Angelopoulou, V.G. Mavramtzas, and D.N. Theodorou, *Atomistic molecular dynamics simulation of diffusion in binary liquid* n*-alkane mixtures*, J. Chem. Phys. 116 (2002), pp. 7656–7665.
[12] E. Hernández and C.R.A. Catlow, *Molecular dynamics simulations of* n*-butane and* n*-hexane diffusion in silicalite*, Proc. R. Soc. Lond. A 448 (1995), pp. 143–160.
[13] F. Kapteijn, J.A. Moulijn, and R. Krishna, *The generalized Maxwell-Stefan model for diffusion in zeolites: sorbate molecules with different saturation loadings*, Chem. Eng. Sci. 55 (2000), pp. 2923–2930.
[14] J. Kärger, S. Vasenkov, and S. Auerbach, *Diffusion in zeolites*, in *Handbook of Zeolite Catalysis and Microporous Materials*, S. Auerbach, K.A. Carrado, and P.K. Dutta, eds., Marcel Dekker, Inc., New York, NY, 2002.
[15] E. Beerdsen, D. Dubbeldam, and B. Smit, *Understanding diffusion in nanoporous materials*, Phys. Rev. Lett. 96 (2006), 044501.
[16] D. Dubbeldam and R.Q. Snurr, *Recent developments in the molecular modeling of diffusion in nanoporous materials*, Mol. Sim. 33 (2007), pp. 305–325.
[17] A.H. Fuchs and A.K. Cheetham, *Adsorption of guest molecules in zeolite materials: computational aspects*, J. Phys. Chem. B 105 (2001), pp. 7375–7383.
[18] J. Rouquerol, D. Avnir, C.W. Fairbridge, D.H. Everett, J.H. Haynes, N. Pernicone, J.D.F. Ramsay, and K.S.W. Sing, *Recommendations for the characterization of porous solids*, Pure Appl. Chem. 66 (1994), pp. 1739–1758.
[19] K.S.W. Sing, D.H. Everett, R.A.W. Haul, L. Moscou, R.A. Pierotti, N. Rouquerol, and T. Siemieniewska, *Reporting physisorption data for gas/solid systems with special reference to the determination of surface area and porosity*, Pure Appl. Chem. 57 (1985), pp. 603–619.
[20] L.D. Gelb, K.E. Gubbins, R. Radhakrishnan, and M. Sliwinska-Bartkowiak, *Phase separation in confined system*, Rep. Porg. Phys. 62 (1999), pp. 1573–1659.
[21] R. Evans, U.M.B. Marconi, and P. Tarazona, *Capillary condensation and adsorption in cylindrical and slit-like pores*, J. Chem. Soc. Faraday Trans. 2 82 (1986), pp. 1763–1787.
[22] P. Tarazona, U.M.B. Marconi, and R. Evans, *Phase equilibria of fluid interfaces and confined fluids*, Mol. Phys. 60 (1987), pp. 573–595.
[23] H. Bock, K.E. Gubbins, and M. Schoen, *Anisotropic self-diffusion in nanofluidic structures*, J. Phys. Chem. C 111 (2007), pp. 15493–15504.
[24] A.V. Neimark, *The method of indeterminate Lagrange multipliers in nonlocal density functional theory*, Langmuir 11 (1995), pp. 4183–4184.
[25] P.I. Ravikovitch and A.V. Neimark, *Density functional theory of adsorption in spherical cavities and pore size characterization of templated nanoporous silicas with cubic and three-dimensional hexagonal structures*, Langmuir 18 (2002), pp. 1550–1560.
[26] B. Coasne, S.K. Jain, L. Naamar, and K.E. Gubbins, *Freezing of argon in ordered and disordered porous carbon*, Phys. Rev. B 76 (2007), 085416.
[27] S.K. Jain, K.E. Gubbins, R.J.M. Pellenq, and J.P. Pikunic, *Molecular modeling and adsorption properties of porous carbons*, Carbon 44 (2006), pp. 2445–2451.
[28] R.L. June, A.T. Bell, and D.N. Theodorou, *Molecular dynamics of butane and hexane in silicalite*, J. Phys. Chem. 96 (1992), pp. 1051–1060.
[29] M.D. Macedonia, D.D. Moore, E.J. Maginn, and M.M. Olken, *Adsorption studies of methane, ethane, and argon in the zeolite mordenite: molecular simulations and experiments*, Langmuir 16 (2000), pp. 3823–3834.
[30] A. Gupta, L.A. Clark, and R.Q. Snurr, *Grand canonical Monte Carlo simulations of nonrigid molecules: siting and segregation in silicalite zeolite*, Langmuir 16 (2000), pp. 3910–3919.

[31] R.L. June, A.T. Bell, and D.N. Theodorou, *Prediction of low occupancy sorption of alkanes in silicalite*, J. Phys. Chem. 94 (1990), pp. 1508–1516.
[32] S.P. Bates, W.J.M. van Well, R.A. van Santen, and B. Smit, *Energetics of* n*-alkanes in zeolites: a configurational-bias Monte Carlo investigation into pore size dependence*, J. Am. Chem. Soc. 118 (1996), pp. 6753–6759.
[33] B. Smit and T.L.M. Maesen, *Molecular simulations of zeolites: adsorption, diffusion, and shape selectivity*, Chem. Rev. 108 (2008), pp. 4125–4184.
[34] E.A. Ustinov, D.D. Do, and V.B. Fenelonov, *Pore size distribution analysis of activated carbons: application of density functional theory using nongraphitized carbon black as a reference system*, Carbon 44 (2006), pp. 653–663.
[35] S. Furmaniak, A.P. Terzyk, P.A. Gauden, K. Lota, E. Frackowiak, F. Beguin, and P. Kowalczyk, *Determination of the space between closed multiwalled carbon nanotubes by GCMC simulation of nitrogen adsorption*, J. Coll. Inter. Sci. 317 (2008), pp. 442–448.
[36] S. Furmaniak, A.P. Terzyk, M. Jaroniec, and P.A. Gauden, *Argon adsorption in channel-like mesoporous carbons at 77 K: grand canonical Monte Carlo simulations and pore size analysis*, Microporous Mesoporous Mater. 116 (2008), pp. 665–669.
[37] B. Smit and C.J.J. den Ouden, *Monte Carlo simulations on the relation between the structure and properties of zeolites: the adsorption of small hydrocarbons*, J. Phys. Chem. 92 (1988), pp. 7169–7171.
[38] C. Baerlocher, L.B. McCusker, and D.H. Olson, *Atlas of Zeolite Framework Types*, Elsevier, Amsterdam, 2007.
[39] K.S.W. Sing and R.T. Williams, *The use of molecular probes for the characterization of nanoporous adsorbents*, Part. Part. Syst. Charact. 21 (2004), pp. 71–79.
[40] B. Smit, *Grand-canonical Monte Carlo simulations of chain molecules: adsorption isotherms of alkanes in zeolites*, Mol. Phys. 85 (1995), pp. 153–172.
[41] B. Smit, *Simulating the adsorption isotherms of methane, ethane, and propane in the zeolite silicalite*, J. Phys. Chem. 99 (1995), pp. 5597–5603.
[42] T.J.H. Vlugt, R. Krishna, and B. Smit, *Molecular simulations of adsorption isotherms for linear and branched alkanes and their mixtures in silicalite*, J. Phys. Chem. B 103 (1999), pp. 1102–1118.
[43] D. Frenkel and B. Smit, *Understanding Molecular Simulation: From Algorithms to Applications*, 2nd ed., Academic Press, San Diego, CA, 2002.
[44] D. Dubbeldam, S. Calero, T.J.H. Vlugt, R. Krishna, T.L.M. Maesen, and B. Smit, *United force field for alkanes in nanoporous materials*, J. Phys. Chem. B 108 (2004), pp. 12301–12313.
[45] T.J.H. Vlugt and M. Schenk, *Influence of framework flexibility on the adsorption properties of hydrocarbons in the zeolite silicalite*, J. Phys. Chem. B 106 (2002), pp. 12757–12763.
[46] E. García-Pérez, J.B. Parra, C.O. Ania, D. Dubbeldam, T.J.H. Vlugt, J.M. Castillo, P.J. Merkling, and S. Calero, *Unraveling the argon adsorption processes in MFI-type zeolite*, J. Phys. Chem. C 112 (2008), pp. 9976–9979.
[47] D.G. Hay and H. Jaeger, *Orthorhombic monoclinic phase-changes in Zsm-5 zeolite silicalite*, J. Chem. Soc. Chem. Commun. 21 (1984), p. 1433.
[48] C.A. Fyfe, H. Strobl, G.T. Kokotailo, G.J. Kennedy, and G.E. Barlow, *Ultra-high-resolution ^{29}Si solid-state MAS NMR investigation of sorbate and temperature-induced changes in the lattice structure of zeolite ZSM-5*, J. Am. Chem. Soc. 110 (1988), pp. 3373–3380.
[49] E.L. Wu, S.L. Lawton, D.H. Olson, A.C. Rohrman, and G.T. Kokotailo, *ZSM-5-type materials. Factors affecting crystal symmetry*, J. Phys. Chem. 83 (1979), pp. 2777–2781.
[50] R.Q. Snurr, A.T. Bell, and D.R. Theodorou, *Prediction of adsorption of aromatic hydrocarbons in silicalite from grand canonical Monte Carlo simulations with biased insertions*, J. Phys. Chem. 97 (1993), pp. 13742–13752.
[51] A.I. Skoulidas and D.S. Sholl, *Transport diffusivities of CH_4, CF_4, He, Ne, Ar, Xe, and SF_6 in silicalite from atomistic simulations*, J. Phys. Chem. B 106 (2002), pp. 5058–5067.
[52] A.V. Kiselev, A.A. Lopatkin, and A.A. Shulga, *Molecular statistical calculation of gas adsorption by silicalite*, Zeolites 5 (1985), pp. 261–267.
[53] B. McEnaney, *Estimation of the dimensions of micropores in active carbons using the Dubinin–Radushkevich equation*, Carbon 25 (1987), pp. 69–75.
[54] A.P. Terzyk, S. Furmaniak, P.A. Gauden, P.J.F. Harris, J. Wloch, and P. Kowalczyk, *Hyper-parallel tempering Monte Carlo simulations of Ar adsorption in new models of microporous non-graphitizing activated carbon: effect of microporosity*, J. Phys. Condens. Matter 19 (2007), 406208.
[55] A.P. Terzyk, S. Furmaniak, P.J.F. Harris, P.A. Gauden, J. Woch, P. Kowalczyk, and G. Rychlicki, *How realistic is the pore size distribution calculated from adsorption isotherms if activated carbon is composed of fullerene-like fragments*, Phys. Chem. Chem. Phys. 9 (2007), pp. 5919–5927.
[56] D.D. Do and H.D. Do, *Pore characterization of carbonaceous materials by DFT and GCMC simulations: a review*, Adsorp. Sci. Tech. 21 (2003), pp. 389–423.
[57] T.J.H. Vlugt, W. Zhu, F. Kapteijn, J.A. Moulijn, B. Smit, and R. Krishna, *Adsorption of linear and branched alkanes in the zeolite silicalite-1*, J. Am. Chem. Soc. 120 (1998), pp. 5599–5600.
[58] T. Maris, T.J.H. Vlugt, and B. Smit, *Simulation of alkane adsorption in the aluminophosphate molecular sieve $AlPO_4$-5*, J. Phys. Chem. B 102 (1998), pp. 7183–7189.
[59] E. García-Pérez, D. Dubbeldam, B. Liu, B. Smit, and S. Calero, *A computational method to characterize framework aluminum in aluminosilicates*, Angew. Chem. Int. Ed. 45 (2006), pp. 276–278.
[60] B. Liu, E. García-Pérez, D. Dubbeldam, B. Smit, and S. Calero, *Understanding aluminum location and non-framework ions effects on alkane adsorption in aluminosilicates: a molecular simulation study*, J. Phys. Chem. C 111 (2007), pp. 10419–10426.
[61] A. Alberti, *Location of Brønsted sites in mordenite*, Zeolites 19 (1997), pp. 411–415.
[62] W.M. Meier, *The crystal structure of mordenite (ptilolite)*, Z. Kristallogr. 115 (1961), pp. 439–450.
[63] M. Pamba, G. Maurin, S. Devautour, J. Vanderschueren, J.C. Giuntini, F.D. Renzo, and F. Hamidi, *Influence of framework Si/Al ratio on the Na^+/mordenite interaction energy*, Phys. Chem. Chem. Phys. 2 (2000), pp. 2027–2031.